TITLE: Time-course Pattern of Cell Degeneration in a Mouse with Cochlear Hair Cell Impaired Potassium Outflow.

Camila Carignano[1,*], Esteban Pablo Barila[1,*], Ezequiel Ignacio Rías[1,2], Leonardo Dionisio[1,2], Eugenio Aztiria[1,2] and Guillermo Spitzmaul[1,2,#]

1. Instituto de Investigaciones Bioquímicas de Bahía Blanca (INIBIBB) – Consejo Nacional de Investigaciones Científicas y Técnicas (CONICET) – Universidad Nacional del Sur (UNS). Camino La Carrindanga Km 7. B8000FWB, Bahía Blanca, Argentina.

2. Departamento de Biología, Bioquímica y Farmacia (BByF) – UNS. San Juan 670, 8000 Bahía Blanca, Argentina.

*** these authors contributed equally to the work.**

To whom correspondence should be addressed: INIBIBB - CONICET/UNS, Camino La Carrindanga Km 7, 8000 Bahía Blanca, Argentina. E-mail: **gspitz@inibibb-conicet.gob.ar**

Abbreviations

OC, organ of Corti; CNS, central nervous system; HCs, hair cells; OHC, outer hair cell; IHC, inner hair cell; SGN, spiral ganglion neuron; WT, wild-type; KO, knock-out; KI, knock-in; *Kcnq4*$^{+/+}$, KCNQ4 WT mice; *Kcnq4*$^{-/-}$: KCNQ4 KO mice; HL, hearing loss; W, postnatal weeks-old; ARHL, age-related hearing loss; NIHL, noise-induced hearing loss; SEM, scanning electron microscopy; S, 5%-length segment;

Abstract

DFNA2 is an inherited and progressive deafness, caused by mutations in a voltage-gated potassium channel, named KCNQ4. Hearing loss develops progressively with age from a mild loss of hearing sensitivity associated with outer hair cell disappearance, to a profound deafness in aged patients, indicating additional mechanisms underlying disease progression. Transgenic mice for KCNQ4 developed loss of outer hair cells which correlates with increased hearing thresholds up to 60 dB, compatible with their amplificatory function.

To get insights into the mechanism of DFNA2 progression, we here associate the analysis of KCNQ4 expression in wild-type mice with cell death rates in a mouse lacking KCNQ4 channel. Expression levels were analyzed by RT-qPCR and mean fluorescence intensity measurements. Next, we investigated inner and outer hair cell degeneration and also examined spiral ganglion neurons survival by plotting cytocochleograms and neuronal counts at different ages, respectively.

We found the highest *Kcnq4* expression in the basal turn, which correlated with outer hair cell degeneration: it is promptly observed in basal turns becoming evident in adjacent turns later, showing different loss rates. Inner hair cell loss develops approximately 35 weeks later, progressing from basal to middle turns. A similar time-course pattern of degeneration was observed for spiral ganglion neurons with a severe loss in basal and apical turns.

These findings suggest that KCNQ4 plays differential roles in each hair cell type, providing new insights into the cellular mechanisms leading to the severe hearing loss suffered by DFNA2 patients in advanced stages.

1. Introduction

Potassium circulation is essential for signal transduction in the hearing process [1, 2], which starts with opening of mechanosensitive cation channels placed at the tips of hair cells [3, 4]. Specialized epithelia on the stria vascularis produce potassium-enriched endolymph that fills in the scala media. To maintain cell homeostasis, once potassium enters hair cells (HCs), it must return to the stria vascularis by exiting HCs and then moving through supporting cells of the organ of Corti (OC). This potassium circulation ensures that the physiological processes of hearing can take place [2, 5]. Alterations in any of the steps involved in this circulation process can generate different kinds of hearing loss [6, 7]. KCNQ4 is the main K^+ channel involved in potassium extrusion from outer hair cells (OHCs). It is a voltage-activated K^+ channel localized at the basal pole of OHCs, generating the $I_{K,n}$ current [8, 9]. Its function is essential for cell survival. Mutations in KCNQ4 cause disruptions on potassium recycling and its consequences are displayed in the DFNA2 deafness [9]. This last is a slow progressive deafness characterized by having two phases in the HL process. The first one starts at around 15-20 years-old exhibiting a mild to moderate HL at high-frequency sounds that progresses over time to middle frequencies [10]. Hearing threshold increases 20 to 60 dB which correlates with a progressive loss of the amplificatory function exerted by OHCs [11]. The second phase is characterized by the progression of HL to a severe impairment by the age of 65-70 [12]. At this stage, hearing threshold increases more than 70-80 dB affecting most of the frequencies and this phenotype cannot be accounted for OHC dysfunction alone [10]. Therefore, other mechanisms must be contributing to the pathology progression. Patients with

this condition are heterozygous for the affected *Kcnq4* allele which bears a point mutation with dominant-negative effect on the tetrameric channel [10, 13]. KCNQ4 channel is not only located in OHCs, but also in inner hear cells (IHCs) and some central nervous system (CNS) nuclei from the brainstem belonging most of them to the auditory pathway [8, 14-16]. For these reasons, it is also believed that IHCs and neurons could also participate in the progression of HL. Many years have passed since the molecular cause of DFNA2 was discovered [13]. However, neither the molecular events gated by KCNQ4 misfunction are fully understood nor the role of IHCs and neurons on disease progression. Research on DFNA2 echoes into the physiology of normal hearing and the comprehension of several hearing pathologies like age-related hearing loss (ARHL), noise-induced hearing loss (NIHL) that share alterations in potassium circulation [7, 10, 17, 18].

Then, in order to understand the contribution of KCNQ4 to potassium homeostasis in the OC we used a KCNQ4 knock-out (KO) mouse that resembles many of the characteristics observed in DFNA2 disease. Remarkably we found that in the absence of KCNQ4, each cochlear cell type is differentially affected, suggesting that the channel plays different roles in each of them. Our results shed light on the cellular mechanisms that would participate in the progression of DFNA2 deafness.

2. Materials and methods

2.1 Animals. C3H/HeJ transgenic mice, lacking the expression of the KCNQ4 protein (*Kcnq4*$^{-/-}$), due to a deletion spanning exon 6 to exon 8, were used [9, 19]. Wild-type (WT) C3H/HeJ litters were used as controls (*Kcnq4*$^{+/+}$) and also C57Bl/6 mice were also used for inter-strain comparison. Mice from both sexes were used in all experiments indistinctly. Age ranges were: a) young mice: 3, 4, 6, 8 and 10 postnatal weeks-old (W); b) middle age adult mice: 40W, 52W, 58W and 60W The experimental protocol followed in this study was approved by the Council for Care and Use of Experimental Animals (CICUAE, protocol N° 083/2016) of the Universidad Nacional del Sur (UNS), whose requirements are strictly based on the European Parliament and Council of the European Union directives (2010/63/EU).

2.2 Tissue preparation. Mice ranging from 3W to 60W were euthanized by CO_2 exposure and inner ears were promptly removed from temporal bones. In order to monitor hair cell and spiral ganglion neuron degeneration, cochleae were studied by immunofluorescence using two different approaches i) mounted as a whole or, ii) in thin tissue sections. Both started with tissue fixation by overnight submersion in 4% paraformaldehyde, washed with PBS, and decalcified using 8-10% EDTA in PBS for up to 5 days depending on animal age, on a rocking shaker at 4°C.

2.2.1 Whole-mount cochlear preparations. The organ of Corti from decalcified cochleae was obtained following a protocol similar to that described in Akil and Lustig, 2013 and Montgomery and Cox, 2016[20, 21]. This method consists in splitting the whole cochlear length into three longitudinal segments: basal, middle and apical turns using fine scissors. Then, the vestibular system, spiral ligament, modiolus and tectorial membrane were removed and the organ of Corti was isolated. Finally, the hook was cut off from the rest of the basal segment.

2.2.2 Modiolar sections. Whole inner ears were processed according to Spitzmaul et al, 2013 and Barclays et al. 2016 [19, 22]. Briefly, after decalcification, inner ears were cryoprotected in 15% sucrose for 4 h, then in 30% sucrose overnight followed by OCT embedding. 10 µm-thick sections, longitudinal to the modiolus, were obtained using a cryostat (Leica CM 1860) and preserved at -20°C until processed.

2.3 Immunofluorescence in whole-mount cochlear preparations. Cochlear turns were postfixed in 4% PFA during 30 min, washed three times in PBS and incubated for 2 h in blocking solution (2% BSA, 0.5% Nonidet P-40 in PBS). Primary antibodies were incubated for 48 h in carrier solution (PBS containing 1% BSA, and 0.25% Nonidet P-40). Subsequently, tissue was rinsed three times in PBS. Secondary antibodies, diluted in carrier solution, were incubated for 2 h at room temperature. After that, samples were washed three times in PBS. Finally, cochlear turns were mounted unflattened in Fluoromount-G (Southern Biotech). The following primary antibodies were used: rabbit anti-KCNQ4 (4) (K4C, 1:200; generously provided by Dr. T. Jentsch, Forschungsinstitut für Molekulare Pharmakologie, Berlin, Germany), goat anti-prestin (1:200, cat#sc-22692, Santa Cruz Biotechnology), rabbit anti-myosin VIIa (1:200, cat#25-6790, Proteus Biosciences). The following fluorescently-labeled secondary antibodies were obtained from Molecular Probes and used diluted (1:500): donkey anti-rabbit 555 (cat#A-31572) and donkey anti-goat 488 (cat#A-11055). Nuclei were stained with DAPI (1:1000).

2.4 Hair cell counting and cytocochleogram plotting. Labeled cells on whole-mount cochleae were imaged using an epifluorescence microscope (Nikon Eclipse E-600) coupled to a CCD camera (Nikon K2E Apogee) and a laser spectral confocal microscope (Leica TCS SP2). Pictures were analyzed using the Image J software and cell counting was carried out manually. HCs were identified based on their tissue localization in the OC. For OHC, row 1 was considered as the innermost cell line followed by row 2 corresponding to the middle line of cells and row 3 to the outermost cell line. Cellular degeneration was evaluated on a cytocochleogram (4-5 animals for each age and genotype). A cytocochleogram is basically a cartographical approach used for determining HC number and distribution along the entire cochlear length [23-26]. It is constructed by plotting the number of OHCs or IHCs versus the relative distance to the apex. In order to normalize the OC´s length, cells were counted separately in 20 segments (S), each of them spanning 5% of the total cochlear length, which was considered the whole (100%) distance. Each S was numbered according to the spanning percentage of the total length, starting from the apex (e.g. from 0% to 5%=S5), to the basal end (S100).

2.5 Cell loss rate estimation. The dynamic of cell loss was calculated plotting the average number of living cells in each segment vs mice age on a logarithmic scale. Data were fitted through the SigmaPlot 12.0 software (Systat Software Inc.) using the Hill equation as follows:

$$N_{OHC} = OHC_{max} \cdot \frac{(Age)^{nH}}{[CD50^{nH} + (Age)^{nH}]}$$

where N_{OHC} represents the number of cells at each age point (in weeks), OHC_{max} is the initial OHC number, CD_{50} is the age where 50% cell death was achieved, and nH is the Hill coefficient that estimates cell death rate.

2.6 Immunofluorescence on cochlear sections. Slide-mounted tissue sections were post fixed with 2% PFA for 20 minutes, washed with PBS and blocked in the same buffer as described in section 2.3. Slice sections were incubated overnight with a primary antibody rabbit anti-beta III Tubulin (tuj1, Covance #mrb-435p) diluted 1:1000 in carrier solution. A fluorescently-labeled goat anti-rabbit 488 (Molecular Probes, cat#A-11034) was used as secondary antibody, which was incubated during 1 h.

2.7 Spiral ganglion neuron density measurements. 10 μm-thick cochlear longitudinal slices, comprising the whole extension of the modiolus, were chosen to perform SGN assessment. Using a 20x magnification objective, fluorescent images were taken for each of the ganglion individual portions (i.e.: basal, medial and apical). Images were processed with Image J's FIJI by demarcating their area and taking into account the bound space of bone surrounding the ganglia and the extent of beta III tubulin staining. Using the cell counter extension of this software, individual cells were counted manually and their density was calculated by dividing the number of SGNs over the area in square micrometers covered by the ganglion. Results were plotted for each portion of the ganglion versus the age, in weeks, for each mouse genotype.

2.8 KCNQ4 signal intensity. The expression pattern of the KCNQ4 channel in OHCs was analyzed on whole-mount cochlear preparations from wild-type mice at different ages. To do so, the organ of Corti was divided into 3 segments, as explained above. To quantify the differences, we measured the mean fluorescence intensity (MFI) of each cell in confocal images using Image J software. For each turn, the intensity of around 20 cells from all 3 rows of OHC in the central area was measured. Background noise was calculated from averaging the signal of 5-6 representative areas where no immunofluorescence was apparent. Specific

signal was calculated by subtracting the averaged background value from that of each immunopositive cell.

2.9 RNA extraction and qPCR. Cochlear RNA was extracted from 3-week-old mice. For each experiment, samples from 3-4 mice were pooled. In brief, immediately after cochlear excision, tissue was immersed in a RNA preservation buffer and then, the vestibular region was removed to keep only the cochlea. Using a scalpel, the cochlea was cut between the first and second turn, in order to obtain a bottom piece containing the basal turn and another one containing the middle and apical turns. RNA was extracted using the TransZol reagent (TransGen Biotech, ET101-01) in combination with Direct-Zol RNA mini prep kit (Zymo Research, R2052), essentially as indicated in Patil et al [27]. cDNA was produced from 500 ng total RNA with EasyScript Reverse Transcriptase (TransGen Biotech Cat #AE101) using anchored oligo (dT)s following manufacturer's indications. Quantitative PCR (qPCR) was carried out using the cDNA generated previously employing the SensiFAST SYBR mix No-Rox Kit (Bioline) in a Rotor-Gene 6000 real-time PCR cycler (Corbett Research). Primers for the *KCNQ4* gene were: 5'-TATGGTGACAAGACGCCACAT-3' (forward) and 5'-GGCAGAAGCACTTTGAGAAGC-3´ (reverse) while for the reference genes were as follows: HPRT 5'-GTTCTTTGCTGACCTGCTGGA-3' (fwd) and 5'-AATGATCAGTCAACGGGGGA-3' (rev); GAPDH 5'-GAGAAACCTGCCAAGTATGATGAC-3' (fwd) and 5'-CCCACTCTTCCACCTTCGAT-3' (rev). Data analysis was done applying the ΔΔCt method [28] to obtain relative mRNA expression.

2.10 Scanning electron microscopy (SEM). Basal cochlear segments were dissected from *Kcnq4*$^{+/+}$ and *Kcnq4*$^{-/-}$ at 4W and 6W. Cochleae were fixed using 2.5% glutaraldehyde for 2 hours and then, decalcified as mentioned previously. Samples were dehydrated with ethanol and a critical point drier was applied. Finally, tissues were imaged with a LEO-EVO 40 XVP-EDS Oxford X-Max 50 scanning electron microscope provided by the Microscopy Facility from Centro Científico Tecnológico – Bahía Blanca (CCT-BB) / CONICET.

2.11 Statistical Analysis. All data and results were confirmed through at least, three independent experiments. Shown values represent the means ± SEM. Significant differences were identified using, i) Student's t-test for experiments shown in Fig. 1A, Fig. 2, Fig. 3B and Fig. 7 and ii) one-way ANOVA, post hoc Tukey Multiple Comparison test for experiments shown in Fig. 1C, Fig. 4 and Fig. 6. Statistical analyses were performed using Excel and SigmaPlot 12.0 Software. Statistical significance is represented with (*) when $p<0.050$; (**) when $p<0.010$ and (***) when $p<0.001$.

3. Results

3.1 Expression of KCNQ4 in cochlea of wild-type mouse.

Previous studies with *Kcnq4* KO allele were performed on mixed background between C57BL/6 and 129/SV mouse strains [9], which should exhibit the broadest range of phenotypes but with incomplete penetrance [29]. In order to display full phenotypes of DFNA2 at both, early and advanced phases, we backcrossed the allele to the C3H/HeJ mouse strain. This strain preserves auditory function up to 15 months of age [30]. For example, when comparing hair cell survival between C3H/HeJ and C57Bl/6 inbred strains at 52W, we obtained a significantly decrease of both HC types in C57Bl/6 strain while they are well preserved in C3H/HeJ strain (Supp. Fig. S1). Thus, C3H/HeJ is a better strain to analyze hair cell loss due to KCNQ4 deletion.

As contradictory KCNQ4 expression profiles have been observed in different mouse strains [9, 14], after allele backcrossing to C3H/HeJ strain, we analyzed KCNQ4 channel expression. KCNQ4 has been reported in the basal membrane of OHCs [8, 9] and also, in IHCs [9, 15]. Using reverse transcription followed by qPCR, we evaluated the expression level of *Kcnq4* mRNA in basal and middle/apical cochlear turns of wild-type mice at 3W. As shown in Fig. 1A, middle/apical turns exhibit around 50% less amounts of *Kcnq4* mRNA compared to the basal turn ($p<0.010$).

The expression of the KCNQ4 protein was evaluated by MFI level measurements performed on cochlear whole-mounts using a primary antibody against KCNQ4 protein [9, 19]. KCNQ4 signal was clearly detected in OHCs (Fig. 1B) while it was absent in IHCs (not shown). Fluorescent signals from the basal, middle and apical turns were separately compared at 3 different ages: 6W, 8W and 10W. Confocal microscopy of KCNQ4-immunostained cochleae showed a strong fluorescence on OHCs in a typical 3-row cell pattern (Fig. 1B). However, although fluorescent signal was robust in OHC of basal and middle turns, it was significantly weaker in cells of the apical turn at all tested ages, suggesting a differential expression pattern. As shown in Fig. 1C, the apical turn exhibits a remarkable decrease of normalized MFI at each age, when compared to basal turn ($p<0.05$ for 6W, 8W and 10W, respectively). For 10W, a significant decrease of normalized MFI (about 20%) was observed for middle turn compared to the basal one ($p<0.05$). Thus, our data suggest a gradient expression of KCNQ4 in OHCs from basal to apical turns.

3.2 Rates of cochlear OHC degeneration along the Organ of Corti.

KCNQ4 channel absence impairs K^+ extrusion from OHCs which would disturb K^+ recycling in the inner ear, leading to OHC death and tissue degeneration [9]. We monitored cell survival in cochlear whole-mount preparations from wild-type and *Kcnq4*$^{-/-}$ mice within an age range from 3W to 58W. OHCs were clearly identified using an anti-prestin antibody (Fig. 2A), which is differentially expressed at the lateral membranes of these cells [9, 19, 31].

Our first approach to this issue showed that for *Kcnq4*$^{+/+}$ mice, cell density did not change significantly with age, while the contrary was observed for *Kcnq4*$^{-/-}$ mice ($p<0.050$) (Fig. 2B). Average cell density for wild-type mice was ~16400±3700 cell/mm^2 (n=5), while *Kcnq4*$^{-/-}$ mice showed an evident decline with age. Cell density for *Kcnq4*$^{-/-}$ was significantly different from wild-type at all age points, being about 25% less at 3-4W, and increasing this difference to 90% at 52W (Fig. 2B, red circle).

In order to understand if these differences could be due to eventual changes in the anatomical structure of the OC, we analyzed its length along the age range under evaluation. In fact, for each mouse genotype, the OC showed no significant differences ($p>0.050$) in length across the studied time frame and also there was no difference between both genotypes (Fig. 2C).

Average length values were 5497±190 µm long (n=24) and 5465±168 µm long (n=26) for *Kcnq4*$^{+/+}$ and *Kcnq4*$^{-/-}$, respectively.

In order to refine our comprehension on the OHC degeneration process exhibited by *Kcnq4*$^{-/-}$ mouse, we used a standard procedure based on cytocochleographic analyses. Fig. 2A depicts an example of a whole-mount OC preparation for a 10W *Kcnq4*$^{-/-}$ mouse. Traversed white dotted lines indicate the boundaries of the 5%-length intervals in which the entire cochlea was divided (see Material and Methods). The absence of OHCs is apparent in basal and middle turns of the OC at this age.

The distribution and abundance of OHCs in each 5%-segment were explored and compared between both mouse genotypes at different ages (Fig. 3A and B). Cytocochleographic analyses of young WT mice (3W-10W) showed an almost constant number of OHCs throughout the cochlea, except for the basal segments (i.e. >90%), where a significant slight decrease in cell number was observed from 4W to 10W ($p<0.05$ from 4-10W) (Fig. 3B, left panel). In middle-age WT mice (40W-58W), OHC survival is similar to that found in young animals within the length range of S20 to S90 (Fig. 3B, left panel). These mice showed as well, a significant reduction in the number of OHCs in apical and basal segments (Fig. 3B, left) ($p<0.05$ for S5, S10, S15 and S100, respectively).

OHC survival is drastically altered in *Kcnq4*$^{-/-}$ mice. At the youngest studied age (3W), OHC number is slightly lower than wild-type until S80, significantly dropping from this point onwards. Within the S85-S100 range, cell number progressively decreases towards the basal segment, developing an 85% OHC loss at the cochlear hook (Fig. 3B, middle panel).

The number of OHCs in *Kcnq4*$^{-/-}$ mice decreases progressively with age across the entire cochlear length, becoming more evident in middle and basal turns (Fig. 3B). While no significant differences were observed between 3W and 4W (Table 1), cell survival gradually decreases becoming significant initially at basal segments (e.g. S95 at 6W), then shifting to more apical segments as age increases (Table 1, Fig. 3B and C). Middle-age adult *Kncq4*$^{-/-}$ mice exhibited a complete absence of OHCs in the basal segments from the S80 forwards. Middle-to-apical segments appear to be less sensitive to the loss of the KCNQ4 protein showing a few remaining OHCs (Fig. 3B, middle panel).

To better describe the impact of OHC disappearance, we calculated the OHC loss ratio between *Kcnq4*$^{-/-}$ and wild-type animals (Fig. 3B, right panel). For the 3W group we observed a slight decrease in cell number that does not reach statistical significance up to S80 when it abruptly increases towards the basal hook. Cell loss ratio extends globally in all segments, with an apparent increased proportion of cell loss in the basal segments due to the initial lower amount of OHCs (Fig. 3B, right panel). Therefore, the velocity of hearing loss seems to speed up from apical to basal segments. Thus, we analyzed the rate of cell loss at each S by plotting the number of OHCs against mice ages (Fig. 3C). While in *Kcnq4*$^{+/+}$ mice, the number of OHCs remains constant over time, it decayed in *Kcnq4*$^{-/-}$ animals. The decay of OHCs was slow at the youngest ages but increases drastically in the following weeks until OHCs complete degenerate at later time points. Most apical S did not follow this pattern, probably due to an overestimation of cell death generated by an age-dependent HL observed also in WT mice (not shown). To describe the kinetic of cell loss we used the Hill equation to fit our temporal data for each S. Fitting slope for apical segments (S15 to S40) was less pronounced than that observed in basal segments (Fig. 3C). In order to visualize the behavior of OHC loss rates, we plotted Hill coefficients and the CD50s obtained from fitted curves for *Kcnq4*$^{-/-}$ mice at each cochlear S (Fig. 3D). Loss rate progressively increases from apical (nH ~0.9) to basal (nH ~2.0) segments in a sigmoidal shape (Fig. 3D). Conversely, we observed that CD50 decreases with increasing distance from the apex, from an initial value of around 22 weeks to a value of 7 weeks at S85 (Fig. 3D). So, the rate of OHC loss is different along cochlear segments, increasing from apex to basal segments.

Then, we thoroughly analyzed cell survival for each of the three OHC rows. Cochleographic studies were carried out in the S20-S60 range for young animals (6W to 10W) since OHC degeneration from these cochlear regions is ongoing within this timeframe, but cell row architecture is still well preserved (Fig. 4A). In wild-type mice, we did not observe differences among OHC counts for each row and around 37 cells/row for each segment was determined (Fig. 4B). In agreement with the results shown above, in *Kcnq4*$^{-/-}$ animals, the OHC number for each row decreases with age (Fig. 4B). However, OHC loss is not equivalent among the three rows. Indeed, the highest decrease was observed for the central row 2. At 6W, only two segments of row 2 showed statistically significant differences respect to the internal row 1 and the external row 3: S25 and S50 ($p<0.05$). The rest of the segments in row 2 exhibited lower cell counts than row 1 and 3, which did not reach statistical significance, suggesting a trend towards higher cell death rate (Fig. 4B, left). At 8W and 10W, differences between row 2 and the others became more evident. Indeed, at 8W and 10W, 5 to 6 segments out of 9 from row 2 showed significant differences (Fig. 4B, middle and right).
Taken together, our results indicate that in *Kcnq4*$^{-/-}$ mice, there is a progressive OHC loss along the entire OC with age but its death rate is not the same throughout the entire cochlear length and the process is not similar among rows.

3.3 OHC stereociliar structure is altered in *Kcnq4*$^{-/-}$ mice.

In order to detect early morphological alterations in OHCs, we also evaluated hair bundle structure of OHCs by SEM in young mice (Fig. 5). Wild-type mice inspection at 4 and 6W (left), showed the characteristic 3-row distribution of OHCs (labeled in the figure as 1, 2 and 3) without spaces between them (Fig. 5A and B). In addition, individual cells bared the typically polarized hair bundle structure, where the upper surface ends up with ordered and neat rows of stereocilia, arranged in a 3-step staircase profile, exhibiting the characteristic W shape (Fig. 5C and D). On the other hand, basal cochlear segments of *Kcnq4*$^{-/-}$ mice, even at 4W, show clear signs of alterations in cell distribution and integrity (Fig. 5, right). The typical 3-row pattern is still recognizable in some regions but not clearly defined in others (Fig. 5E and F). Cell degeneration becomes apparent at this age because several hair bundles are missing and were replaced by scars on tissue surface. OHC loss is even greater at 6W (see white arrows in Fig. 5E and F), being these results in agreement with those described above (see Fig. 3). In addition, hair bundle structure exhibited evident damage showing a disorganized pattern (Fig. 5G and H). The most frequent alteration observed in hair bundles was the tip-fusion of the 3 stereociliar rows (see asterisks in Fig. 5E-H), which can span from small to big portions of the bundle. In some cases, a fusion between two different bundles could be observed. Fig. 5 allows identifying several steps of the fusion process, starting from the fusion of individual and still recognizable stereocilia (asterisks), progressing to “walls” of fused stereocilia (yellow arrowhead) in which, individual stereocilia are no longer recognizable. Occasionally, it was also possible to observe floppy stereocilia (white arrowhead). So, in agreement with previous data, high resolution pictures showed several steps of degenerating OHCs. The observed alterations in hair bundle structures must affect cell function and contribute to hearing impairment before cell death and replacement by supporting cells on OC surface.

3.4 Degeneration of IHCs proceeds later than OHCs.

As we did for the OHC degeneration study, we also used cytocochleographic analysis to evaluate IHC degeneration from WT and KO mice. To do so, we evaluated IHC survival in young and middle-age adults. *Kcnq4*$^{+/+}$ mice showed a mean number of around 33 IHC/S, remaining constant across the S10 to S80 cochlear length range for all ages. However, in basal segments (i.e. >S80), the number of IHCs was statistically lower at all ages ($p<0.05$)

(Fig. 6B, left panel). On the contrary, in *Kcnq4*$^{-/-}$ mice each age showed different IHC counts along the cochlea. Indeed, while in younger mice (10W) the number of IHC remained practically constant and similar to wild-type animals throughout the entire cochlear length, middle-age adult mice showed a strong decrease of IHC number in basal turns. 40W animals display differences that reach significance from S80 onwards ($p<0.05$), showing a 60% decrease in cell number, respect to the apical segments. From this age forwards, IHC loss exhibited a time-dependent increase in cell loss progressing from basal to middle turns (Fig. 6B). Indeed, at S75, IHC counts became lower than 10 cells/S reaching a complete IHC loss in basal segments (>S95) ($p<0.05$). Additionally, 58W animals evidenced cell loss in segments closer to the apex that is not observed in wild-type mice.
We also determined the cell number ratio between wild-type and KO animals. Fig. 6B (right panel) exhibits that IHC loss starts slightly at S55-S60 and progresses considerably towards basal segments in middle-age mice.
Collectively, our results show that IHC death in KO mice also progresses with age, however, this process appears to be subtler than the one observed for OHC, since IHC death starts afterward.

3.5 Spiral ganglion neurons are also affected by KCNQ4 channel absence.

We also analysed SGN survival in mice lacking KCNQ4 channel expression on cochlear sections. SGN density was determined for basal, middle and apical segments of the spiral ganglia at different ages, using slices longitudinal to the modiolus which display the three cochlear turns (Fig. 7A). *Kcnq4*$^{+/+}$ mice exhibited an average value of 36-39 neurons/0.01mm^2 for the three cochlear segments at 15W. This value remains practically constant through age for the different segments (Fig. 7B and C). On the contrary, in *Kcnq4*$^{-/-}$ animals, we determined a neuronal loss that varies differentially with ganglion localization (Fig. 7A). A clear neuronal loss is seen in basal and apical turns in KO mice older than 1 year (Fig. 7B). Neuron density gradually decreases for basal and apical turns as mice grow old, while for middle segments remains almost invariable (Fig. 7C). Although a great variability was obtained for neuronal density measurement due to unevenness in cochlear slices, a clear tendency to a decrease in neuronal counts was observed at 40W in the basal segment that increases with age, reaching a 60% neuronal loss at 60W mice ($p<0.05$) (Fig. 7C). Apical neurons from *Kcnq4*$^{-/-}$ mice also degenerate although differences become significant only at 1-year-old ($p<0.05$) (Fig. 7C). For middle segments, neurons are well preserved showing similar counts to wild-type mice up to 60W (Fig. 7A and C).
In summary, in *Kcnq4*$^{-/-}$ mice, SGNs also degenerate, but later than OHCs and timely-tuned to IHC loss. However, a main difference with HC degeneration is that SGN loss is noticeable in apical segments and that middle segment neurons are well preserved through the entire lifespan.

4. Discussion

4.1. DFNA2 hearing loss and KCNQ4 channel expression.

We constructed cartographical maps of cellular degeneration in cochlear hair cells and neurons using the C3H/HeJ mouse strain. The original characterization was performed on a mixed background and IHC loss was not detected in *Kcnq4* KO mouse, even in animals older than 1 year [9]. In C3H/HeJ wild-type mice, cochlear expression of KCNQ4 was detected only in OHCs, in accordance with Kharkovets et al 2006 and others [9, 32-36]. Expression was higher in basal than apical turns at both, mRNA and protein level [9, 14]. Our results showed a decreasing gradient of KCNQ4 expression from basal to apical turns in young adult mice. This is in agreement with previous data obtained in different mouse backgrounds and

the $I_{K,n}$ current magnitudes obtained in guinea pig [9, 37]. These findings correlate with the reduction of hearing sensitivity at high frequencies during early stages in DFNA2 [10]. Also, ototoxic drugs that alter KCNQ4 channel function also exhibit a similar degenerative profile, where OHCs from basal turns are more sensitive to their deleterious effects [38-40]. However, this expression pattern differs from that reported by others. Beisel et al [14] found that KCNQ4 is highly expressed in OHCs from the apical turn, decreasing towards the basal hook. Besides, they detected expression of KCNQ4 in IHCs and SGNs, which was higher in basal than apical turns. By contrast, our IF experiments could not detect KCNQ4 expression neither in IHCs nor SGNs. The reason for these differences is not clear, considering that the same epitope was recognized by the primary antibody. Differences could be due to mice genetic backgrounds employed in each case. This is an important issue, since several mouse backgrounds undergo ARHL [41], such as the C57Bl/6 strain, due to the presence of the *Ahl* allele or others [42]. Our analysis of inbred C57Bl/6 exhibited a decrease of both HCs in basal and middle segments of the OC at 1-year-old mice (see Suppl. Fig. 1), which in our study would overestimate cell death. The C3H/HeJ mouse background offers several advantages for our studies over other strains because: i) the expression pattern of KCNQ4 is the most reported among different mouse strains and other species (rat, guinea pig); and ii) cell survival is very high, even at advanced ages, keeping age-related hair cell death to a minimum [30]. Thus, the survival measurement determined in our study better reflects the one generated by KCNQ4 channel absence.

Although we could not detect expression of KCNQ4 in IHCs or SGNs, several other experimental approaches suggest its expression in IHCs, including the mouse model used in this study [9, 15, 43]. Channel expression seems to be restricted to the neck of the IHC, along with BK channel [15]. KCNQ4 is responsible for the $I_{K,n}$ current observed in IHCs contributing to restore membrane potential since its absence generates a slight depolarization [9, 14, 15, 43]. Concerning to SGNs, KCNQ4 expression was reported by Beisel et al (2000), predominantly in basal turns. This KCNQ4 expression pattern was coincident with those observed for IHCs [14, 16]. Also, Kv7 currents had been detected in SGNs [44]. Blockade of this currents by linopirdine had a more pronounced apoptotic effect over basal than apical SGNs. Expression of KCNQ4 channels in these cells may be involved in their survival, as determined in our study.

4.2. Rate of OHC death.

We constructed cytocochleograms for OHC survival at different ages. This tool enables not only cell count normalization throughout the entire age frame under study, but also it allows to compare HL among species (e.g. humans)[26]. Our spatiotemporal analysis revealed that all segments develop OHC degeneration, although at different rates. Surprisingly by week 3, basal segments already showed cell loss. As this was the youngest age tested, we assume OHC degeneration had already begun, considering that KCNQ4 channel is not required for OHC differentiation or maturation and that its localization in the rest of OHCs exhibited the mature profile [36]. However, we cannot exclude a developmental or maturational defect of OHC which is taking place before the onset of hearing by P10-12 [36, 45]. Cell survival was tracked during several weeks in young and middle-age animals allowing us to determine cell death rate for each segment. From these data, we observed that the basal turn showed the highest rate while for the apical turn was the opposite. When we plotted cell survival for each segment as a function of age, we observed that cell loss was not linear in any cochlear segment. Considering that OHCs from KO and KI mouse models for KCNQ4 are chronically depolarized [9], our results suggest that at the initial steps of the pathology, OHCs are able to endure the altered resting membrane potential for some weeks before start dying abruptly. Interestingly, the rates for cell death are not uniform. To obtain rate trends we fitted our data

with the Hill equation and found that basal turns had a cell loss $(Age)^2$ times faster than the apical turns. Our data is in agreement to the differential rates observed in DFNA2 patients where hearing loss is faster for high- than for low frequency sounds [10]. Although the progression of cell loss in KO mouse is much faster than that observed in heterozygous KI mouse [9], our results support this disease progression. In consequence, our data indicate that the expression level of KCNQ4 is relevant to the extrusion function of OHCs because there is a direct correlation between channel expression levels and cell death kinetics.

We also go deeper into the analysis and determined that OHC rows differentially degenerate during the process. Although most OHCs die, the middle row showed a significantly higher proportion of cell death trough time. The contribution of individual OHC rows to hearing has not been clearly established yet. Modeling predictions indicate that hearing amplification requires all three rows of OHCs. However, a controlled exposure to styrene that produces a specific loss of the outer row had no significant effect on cochlear sensitivity [46, 47]. Although we have not measured the functional properties of OHCs, our data predicts a deterioration of hearing sensitivity in several regions of the OC. It is noteworthy that we also found stereociliar alterations in basal turns of young KCNQ4 KO mice, suggesting an impaired function at early stages in basal turn. Electron microscopy pictures in young mice indicated that cell rows are still recognizable in some regions, but several OHCs were replaced by scars. Several stereociliar alterations are present in KO mice whose features resemble those identified in NIHL, due to OHC overstimulation [48, 49]. Thus, chronic depolarization of OHCs would keep mechanical work exerted by prestin constantly active in a similar way to high-sound exposure leading to cell overstimulation [50]. In consequence, both pathologies would share several features leading to HL. Hence, KCNQ4 KO mouse would be a good model to investigate molecular mechanisms and to test drugs to help or prevent NIHL. Besides, *Kcnq4* gene polymorphisms have been associated with ARHL [51]. Therefore, alteration in KCNQ4 channel function could also be related with the subtle and slow progressive hearing impairment observed in ARHL. Sustained depolarization of cell membrane would pose continuous cellular stress that, depending on its intensity will gate cell death sooner or later. In consequence, a better comprehension on the molecular mechanisms involved in KCNQ4 channel function would impact in our understanding of this disease and its treatment.

4.3. IHC and SGN degeneration in mouse lacking KCNQ4 channel expression.

Additionally to OHC degeneration, we also determined loss of IHCs and SGNs that was previously not observed in KI or KO KNCQ4 mice using another strain [9]. However, these cells die much later than OHCs. In our experiments, we detected a significant IHC death by week 40 restricted to basal turn. The pattern of cell death progression is slightly different than OHCs because it moves from basal to middle regions. The proportion of cell loss is very high in basal regions where the presence of IHCs was not detected at all after 40W. Cell loss progresses with age moving to the middle turn. Additionally, 1 year-old mice had a slight but significant decrease in cell survival in the most apical segments (around 30%). Thus, this data indicates that middle-age adult KO mice in the C3H/HeJ strain, will suffer from a deep HL to high-frequency sounds. KCNQ4 channel expression has been detected in IHCs contributing to determine resting membrane potential [14, 15, 43]. Mature IHCs exhibit three main potassium currents, named $I_{K,f}$, $I_{K,s}$ and $I_{K,n}$ carried out by BK, an still unknown Kv channel and KCNQ4 channel, respectively [9, 43, 52, 53]. KCNQ4/$I_{K,n}$ is active at resting potential and would not be involved in the main potassium extrusion mechanism. Then, it becomes more important at membrane potentials lower than -50 to -60 mV, setting resting membrane potential. In consequence, lack of KCNQ4 expression generates a slighter membrane depolarization when

compared to OHCs [9]. Our results suggest KCNQ4 channel is also necessary for long term IHC survival but this depolarization would have a less deleterious effect than in OHCs. The significance of $I_{K,n}$ would impact differentially on the lifespan of each hair cell type.

We also found loss of SGNs, starting in middle-age adults, mostly in parallel with IHC loss. Similarly, it progresses from basal turns. Although the analysis for SGNs was not so detailed due to technical limitations, we detected a strong reduction in the number of neurons. There was a decay of neuronal density in apical regions, suggesting a link between IHC and SGN death. M-current, generated by KCNQ channels has been detected in SGNs [44], and KCNQ4 channel expression was also noticed [14]. However, KCNQ2 and KCNQ3 subunits were also reported in SGNs [54]. Then, the molecular composition of the M-current detected in these studies cannot be ascribed to KCNQ4 channel and we cannot assert the possibility of cell death due to the lack of this channel. It is still unknown whether neuronal degeneration in KO mouse occurs as a primary event due to KCNQ4 absence or if it is a consequence of IHC loss. There is evidence indicating that SGN survival depends on trophic support provided by IHCs [55] and supporting cells [56-58]. Our data suggests that the absence of IHCs impacts on SGN viability. However, as we did not analyse supporting cell survival, we cannot rule out the participation of this cell in this process. Additionally, synaptic disconnection between IHC and SGN has been postulated as an earlier event triggering neuron degeneration [59]. However, electron microscopy pictures from KCNQ4 KO mice revealed an intact synaptic connection [9]. In summary, SGN death is a later event in mouse lacking KNCQ4 expression and its cause cannot be certainly attributed to this channel function, but probably to IHC disappearance.

IHC and SGN loss was not detected in the previous study from Kharkovets et al (2006) using the same allele but in a mixed mice strain. ABR measurements were performed stimulating cochlear function with low frequency sounds (5.5 kHz) up to 60W, which must activate hair cells from apical turns. In these conditions, only an increase in hearing threshold of about 60 dB was detected which is compatible with a loss of OHCs. In our study, middle-age adult mice had only a slight decrease of IHC counts at this frequency (corresponding to S5) which would be compatible with these measurements. However, we obtain a strong IHC death in basal turns at the same period that was not seen in Kharkovets et al (2006). Genetic background carried by different mouse strains can modulate the expression pattern of certain phenotypes even when they carry the same mutant allele [29, 60]. These effects have been observed in *Kcnq2* and *Kcnq3* KI mice whose seizure susceptibility exhibited differences, depending not only on the sex and age, but also on the mice strain [61, 62]. Therefore, our results could be ascertained to interstrain differences in genetic background that alter phenotype expressivity. Mixed backgrounds are recommended for initial studies on transgenic mice to obtain the strongest phenotypes which are not dependent on modifier genes expressed in specific inbred strains [29]. However, for some transgenic mice, full phenotypes due to protein modification can be observed only in inbred strains, as in our case. The effect of modifier genes also has been observed in human patients of DFNA2 as differences in HL progression not only due to different mutations but also in families carrying the same mutation [10, 12].

5. Conclusions

Our results provide evidence to explain the progression of human DFNA2 from its initial steps to the profound deafness observed in aged patients (older than 70 years-old). The early stage of HL is compatible with progressive OHC death from basal to apical turns and the later stage correlates with IHC and SGN disappearance. Our data showed that all cells involved in the initial steps of sound transduction are differentially affected by KCNQ4 absence, posing the intriguing possibility of a neuronal contribution on the progression of hearing loss.

Acknowledgments

Our special thanks to Prof. Thomas Jentsch (Max-Delbrück-Centrum für Molekulare Medizin and Leibniz-Institut für Molekulare Pharmakologie, Berlin, Germany) for generously providing *Kcnq4*$^{-/-}$ animals. This work was supported by grants from Agencia Nacional de Promoción Científica y Tecnológica (PICT 2016 N°0260) and Universidad Nacional del Sur (PGI N°24/B262) to GS.

Conflict of Interest Statement

The authors declared that this work was performed in the absence of conflict of interest.

References

[1] A.A. Zdebik, P. Wangemann, T.J. Jentsch, Potassium ion movement in the inner ear: insights from genetic disease and mouse models, Physiology, 24 (2009) 307-316. https://doi.org/10.1152/physiol.00018.2009

[2] H. Hibino, Y. Kurachi, Molecular and physiological bases of the K^+ circulation in the mammalian inner ear, Physiology, 21 (2006) 336-345. https://doi.org/10.1152/physiol.00023.2006

[3] B. Pan, N. Akyuz, X.P. Liu, Y. Asai, C. Nist-Lund, K. Kurima, B.H. Derfler, B. Gyorgy, W. Limapichat, S. Walujkar, L.N. Wimalasena, M. Sotomayor, D.P. Corey, J.R. Holt, TMC1 Forms the Pore of Mechanosensory Transduction Channels in Vertebrate Inner Ear Hair Cells, Neuron, 99 (2018) 736-753 e736. https://doi.org/10.1016/j.neuron.2018.07.033

[4] K. Kurima, S. Ebrahim, B. Pan, M. Sedlacek, P. Sengupta, B.A. Millis, R. Cui, H. Nakanishi, T. Fujikawa, Y. Kawashima, B.Y. Choi, K. Monahan, J.R. Holt, A.J. Griffith, B. Kachar, TMC1 and TMC2 Localize at the Site of Mechanotransduction in Mammalian Inner Ear Hair Cell Stereocilia, Cell Rep, 12 (2015) 1606-1617. https://doi.org/10.1016/j.celrep.2015.07.058

[5] P. Mistrik, J. Ashmore, The role of potassium recirculation in cochlear amplification, Curr Opin Otolaryngol Head Neck Surg, 17 (2009) 394-399. https://doi.org/10.1097/MOO.0b013e328330366f

[6] F. Lang, V. Vallon, M. Knipper, P. Wangemann, Functional significance of channels and transporters expressed in the inner ear and kidney, Am J Physiol Cell Physiol, 293 (2007) C1187-1208. https://doi.org/10.1152/ajpcell.00024.2007

[7] L. Van Laer, P.I. Carlsson, N. Ottschytsch, M.L. Bondeson, A. Konings, A. Vandevelde, N. Dieltjens, E. Fransen, D. Snyders, E. Borg, A. Raes, G. Van Camp, The contribution of genes involved in potassium-recycling in the inner ear to noise-induced hearing loss, Hum Mutat, 27 (2006) 786-795. https://doi.org/10.1002/humu.20360

[8] T. Kharkovets, J.P. Hardelin, S. Safieddine, M. Schweizer, A. El-Amraoui, C. Petit, T.J. Jentsch, KCNQ4, a K^+-channel mutated in a form of dominant deafness, is expressed in the inner ear and the central auditory pathway, Proc Natl Acad Sci U S A, 97 (2000) 4333-4338. https://doi.org/10.1073/pnas.97.8.4333

[9] T. Kharkovets, K. Dedek, H. Maier, M. Schweizer, D. Khimich, R. Nouvian, V. Vardanyan, R. Leuwer, T. Moser, T.J. Jentsch, Mice with altered KCNQ4 K^+ channels implicate sensory outer hair cells in human progressive deafness, Embo J, 25 (2006) 642-652. https://doi.org/10.1038/sj.emboj.7600951

[10] L.M. Dominguez, K.M. Dodson, Genetics of hearing loss: focus on DFNA2, Appl Clin Genet, 5 (2012) 97-104. https://doi.org/10.2147/TACG.S35525

[11] L. Nie, KCNQ4 mutations associated with nonsyndromic progressive sensorineural hearing loss, Curr Opin Otolaryngol Head Neck Surg, 16 (2008) 441-444. https://doi.org/10.1097/moo.0b013e32830f4aa3

[12] E.M. De Leenheer, R.J. Ensink, H.P. Kunst, H.A. Marres, Z. Talebizadeh, F. Declau, S.D. Smith, S. Usami, P.H. Van de Heyning, G. Van Camp, P.L. Huygen, C.W. Cremers, DFNA2/KCNQ4 and its manifestations, Adv Otorhinolaryngol, 61 (2002) 41-46. https://doi.org/10.1159/000066802

[13] C. Kubisch, B.C. Schroeder, T. Friedrich, B. Lütjohann, A. El-Amraoui, S. Marlin, C. Petit, T.J. Jentsch, KCNQ4, a novel potassium channel expressed in sensory outer hair cells, is mutated in dominant deafness, Cell, 96 (1999) 437-446. https://doi.org/10.1016/s0092-8674(00)80556-5

[14] K.W. Beisel, S.M. Rocha-Sanchez, K.A. Morris, L. Nie, F. Feng, B. Kachar, E.N. Yamoah, B. Fritzsch, Differential expression of KCNQ4 in inner hair cells and sensory neurons is the basis of progressive high-frequency hearing loss, J Neurosci, 25 (2005) 9285-9293. https://doi.org/10.1523/JNEUROSCI.2110-05.2005

[15] D. Oliver, M. Knipper, C. Derst, B. Fakler, Resting potential and submembrane calcium concentration of inner hair cells in the isolated mouse cochlea are set by KCNQ-type potassium channels, J Neurosci, 23 (2003) 2141-2149. https://doi.org/10.1523/jneurosci.23-06-02141.2003

[16] K.W. Beisel, N.C. Nelson, D.C. Delimont, B. Fritzsch, Longitudinal gradients of KCNQ4 expression in spiral ganglion and cochlear hair cells correlate with progressive hearing loss in DFNA2, Brain Res Mol Brain Res, 82 (2000) 137-149. https://doi.org/10.1016/s0169-328x(00)00204-7

[17] A.C. Wong, A.F. Ryan, Mechanisms of sensorineural cell damage, death and survival in the cochlea, Front Aging Neurosci, 7 (2015) 58. https://doi.org/10.3389/fnagi.2015.00058
[18] E. Fransen, N. Lemkens, L. Van Laer, G. Van Camp, Age-related hearing impairment (ARHI): environmental risk factors and genetic prospects, Exp Gerontol, 38 (2003) 353-359. https://doi.org/10.1016/s0531-5565(03)00032-9
[19] G. Spitzmaul, L. Tolosa, B.H. Winkelman, M. Heidenreich, M.A. Frens, C. Chabbert, C.I. de Zeeuw, T.J. Jentsch, Vestibular role of KCNQ4 and KCNQ5 K^+ channels revealed by mouse models, J Biol Chem, 288 (2013) 9334-9344. https://doi.org/10.1074/jbc.m112.433383
[20] S.C. Montgomery, B.C. Cox, Whole Mount Dissection and Immunofluorescence of the Adult Mouse Cochlea, J Vis Exp, (2016). https://doi.org/10.3791/53561
[21] O. Akil, L.R. Lustig, Mouse Cochlear Whole Mount Immunofluorescence, in: Bio-protocol, vol. 3, 2013, pp. e332. http://www.bio-protocol.org/e332 https://doi.org/10.21769/bioprotoc.332
[22] M. Barclay, A.F. Ryan, G.D. Housley, Type I vs type II spiral ganglion neurons exhibit differential survival and neuritogenesis during cochlear development, Neural Dev, 6 (2011) 33. https://doi.org/10.1186/1749-8104-6-33
[23] L. Sanz, S. Murillo-Cuesta, P. Cobo, R. Cediel-Algovia, J. Contreras, T. Rivera, I. Varela-Nieto, C. Avendano, Swept-sine noise-induced damage as a hearing loss model for preclinical assays, Front Aging Neurosci, 7 (2015) 7. https://doi.org/10.3389/fnagi.2015.00007
[24] R.W. Boyce, K.A. Dorph-Petersen, L. Lyck, H.J. Gundersen, Design-based stereology: introduction to basic concepts and practical approaches for estimation of cell number, Toxicol Pathol, 38 (2010) 1011-1025. https://doi.org/10.1177/0192623310385140
[25] M. Muller, K. von Hunerbein, S. Hoidis, J.W. Smolders, A physiological place-frequency map of the cochlea in the CBA/J mouse, Hear Res, 202 (2005) 63-73. https://doi.org/10.1016/j.heares.2004.08.011
[26] A. Viberg, B. Canlon, The guide to plotting a cochleogram, Hear Res, 197 (2004) 1-10. https://doi.org/10.1016/j.heares.2004.04.016
[27] K. Vikhe Patil, B. Canlon, C.R. Cederroth, High quality RNA extraction of the mammalian cochlea for qRT-PCR and transcriptome analyses, Hear Res, 325 (2015) 42-48. https://doi.org/10.1016/j.heares.2015.03.008
[28] K.J. Livak, T.D. Schmittgen, Analysis of relative gene expression data using real-time quantitative PCR and the 2(-Delta Delta C(T)) Method, Methods, 25 (2001) 402-408. https://doi.org/10.1006/meth.2001.1262
[29] T. Doetschman, Influence of genetic background on genetically engineered mouse phenotypes, Methods Mol Biol, 530 (2009) 423-433. https://doi.org/10.1007/978-1-59745-471-1_23
[30] D.R. Trune, J.B. Kempton, C. Mitchell, Auditory function in the C3H/HeJ and C3H/HeSnJ mouse strains, Hear Res, 96 (1996) 41-45. https://doi.org/10.1016/0378-5955(96)00017-2
[31] P. Dallos, Cochlear amplification, outer hair cells and prestin, Curr Opin Neurobiol, 18 (2008) 370-376. https://doi.org/10.1016/j.conb.2008.08.016
[32] M. Mustapha, Q. Fang, T.W. Gong, D.F. Dolan, Y. Raphael, S.A. Camper, R.K. Duncan, Deafness and permanently reduced potassium channel gene expression and function in hypothyroid Pit1dw mutants, J Neurosci, 29 (2009) 1212-1223. https://doi.org/10.1523/JNEUROSCI.4957-08.2009
[33] H. Winter, C. Braig, U. Zimmermann, H.S. Geisler, J.T. Franzer, T. Weber, M. Ley, J. Engel, M. Knirsch, K. Bauer, S. Christ, E.J. Walsh, J. McGee, I. Kopschall, K. Rohbock, M. Knipper, Thyroid hormone receptors TRalpha1 and TRbeta differentially regulate gene expression of Kcnq4 and prestin during final differentiation of outer hair cells, J Cell Sci, 119 (2006) 2975-2984. https://doi.org/10.1242/jcs.03013
[34] L. Ruttiger, M. Sausbier, U. Zimmermann, H. Winter, C. Braig, J. Engel, M. Knirsch, C. Arntz, P. Langer, B. Hirt, M. Muller, I. Kopschall, M. Pfister, S. Munkner, K. Rohbock, I. Pfaff, A. Rusch, P. Ruth, M. Knipper, Deletion of the Ca^{2+}-activated potassium (BK) α-subunit but not the BKβ1-subunit leads to progressive hearing loss, Proc Natl Acad Sci U S A, 101 (2004) 12922-12927. https://doi.org/10.1073/pnas.0402660101

[35] M. Jaumann, J. Dettling, M. Gubelt, U. Zimmermann, A. Gerling, F. Paquet-Durand, S. Feil, S. Wolpert, C. Franz, K. Varakina, H. Xiong, N. Brandt, S. Kuhn, H.S. Geisler, K. Rohbock, P. Ruth, J. Schlossmann, J. Hutter, P. Sandner, R. Feil, J. Engel, M. Knipper, L. Ruttiger, cGMP-Prkg1 signaling and Pde5 inhibition shelter cochlear hair cells and hearing function, Nat Med, 18 (2012) 252-259. https://doi.org/10.1038/nm.2634
[36] S. Takahashi, W. Sun, Y. Zhou, K. Homma, B. Kachar, M.A. Cheatham, J. Zheng, Prestin Contributes to Membrane Compartmentalization and Is Required for Normal Innervation of Outer Hair Cells, Front Cell Neurosci, 12 (2018) 211. https://doi.org/10.3389/fncel.2018.00211
[37] F. Mammano, J.F. Ashmore, Differential expression of outer hair cell potassium currents in the isolated cochlea of the guinea-pig, J Physiol, 496 (Pt 3) (1996) 639-646. https://doi.org/10.1113/jphysiol.1996.sp021715
[38] A.M. Sheppard, G.D. Chen, R. Salvi, Potassium ion channel openers, Maxipost and Retigabine, protect against peripheral salicylate ototoxicity in rats, Hear Res, 327 (2015) 1-8. https://doi.org/10.1016/j.heares.2015.04.007
[39] M.G. Leitner, C.R. Halaszovich, D. Oliver, Aminoglycosides Inhibit KCNQ4 Channels in Cochlear Outer Hair Cells via Depletion of Phosphatidylinositol(4,5)bisphosphate, Molecular Pharmacology, 79 (2011) 51-60. https://doi.org/10.1124/mol.110.068130
[40] S.A. Fausti, B.Z. Rappaport, M.A. Schechter, R.H. Frey, T.T. Ward, R.E. Brummett, Detection of aminoglycoside ototoxicity by high-frequency auditory evaluation: selected case studies, Am J Otolaryngol, 5 (1984) 177-182. https://doi.org/10.1016/s0196-0709(84)80009-5
[41] K.L. Kane, C.M. Longo-Guess, L.H. Gagnon, D. Ding, R.J. Salvi, K.R. Johnson, Genetic background effects on age-related hearing loss associated with Cdh23 variants in mice, Hear Res, 283 (2012) 80-88. https://doi.org/10.1016/j.heares.2011.11.007
[42] M.R. Bowl, S.J. Dawson, The mouse as a model for age-related hearing loss - a mini-review, Gerontology, 61 (2015) 149-157. https://doi.org/10.1159/000368399
[43] W. Marcotti, S.L. Johnson, M.C. Holley, C.J. Kros, Developmental changes in the expression of potassium currents of embryonic, neonatal and mature mouse inner hair cells, J Physiol, 548 (2003) 383-400. https://doi.org/10.1113/jphysiol.2002.034801
[44] P. Lv, D. Wei, E.N. Yamoah, Kv7-type channel currents in spiral ganglion neurons: involvement in sensorineural hearing loss, J Biol Chem, 285 (2010) 34699-34707. https://doi.org/10.1074/jbc.M110.136192
[45] A.V. Bulankina, T. Moser, Neural circuit development in the mammalian cochlea, Physiology (Bethesda), 27 (2012) 100-112. https://doi.org/10.1152/physiol.00036.2011
[46] M. Murakoshi, S. Suzuki, H. Wada, All Three Rows of Outer Hair Cells Are Required for Cochlear Amplification, Biomed Res Int, 2015 (2015) 727434. https://doi.org/10.1155/2015/727434
[47] G.D. Chen, C. Tanaka, D. Henderson, Relation between outer hair cell loss and hearing loss in rats exposed to styrene, Hear Res, 243 (2008) 28-34. https://doi.org/10.1016/j.heares.2008.05.008
[48] R.V. Harrison, The prevention of noise induced hearing loss in children, Int J Pediatr, 2012 (2012) 473541. https://doi.org/10.1155/2012/473541
[49] N. Slepecky, Overview of mechanical damage to the inner ear: noise as a tool to probe cochlear function, Hear Res, 22 (1986) 307-321. https://doi.org/10.1016/0378-5955(86)90107-3
[50] A. Kao, S.W. Meenderink, D. Bozovic, Mechanical overstimulation of hair bundles: suppression and recovery of active motility, PLoS One, 8 (2013) e58143. https://doi.org/10.1371/journal.pone.0058143
[51] E. Van Eyken, L. Van Laer, E. Fransen, V. Topsakal, N. Lemkens, W. Laureys, N. Nelissen, A. Vandevelde, T. Wienker, P. Van De Heyning, G. Van Camp, KCNQ4: a gene for age-related hearing impairment?, Hum Mutat, 27 (2006) 1007-1016. https://doi.org/10.1002/humu.20375
[52] S.L. Johnson, Membrane properties specialize mammalian inner hair cells for frequency or intensity encoding, Elife, 4 (2015). https://doi.org/10.7554/eLife.08177
[53] S.J. Pyott, A.L. Meredith, A.A. Fodor, A.E. Vazquez, E.N. Yamoah, R.W. Aldrich, Cochlear function in mice lacking the BK channel alpha, beta1, or beta4 subunits, J Biol Chem, 282 (2007) 3312-3324. https://doi.org/10.1074/jbc.M608726200

[54] Z. Jin, G.H. Liang, E.C. Cooper, L. Jarlebark, Expression and localization of K channels KCNQ2 and KCNQ3 in the mammalian cochlea, Audiol Neurootol, 14 (2009) 98-105. https://doi.org/10.1159/000158538
[55] L.N. Gillespie, R.K. Shepherd, Clinical application of neurotrophic factors: the potential for primary auditory neuron protection, Eur J Neurosci, 22 (2005) 2123-2133. https://doi.org/10.1111/j.1460-9568.2005.04430.x
[56] M. Sugawara, J.C. Murtie, K.M. Stankovic, M.C. Liberman, G. Corfas, Dynamic patterns of neurotrophin 3 expression in the postnatal mouse inner ear, J Comp Neurol, 501 (2007) 30-37. https://doi.org/10.1002/cne.21227
[57] M. Sugawara, G. Corfas, M.C. Liberman, Influence of supporting cells on neuronal degeneration after hair cell loss, J Assoc Res Otolaryngol, 6 (2005) 136-147. https://doi.org/10.1007/s10162-004-5050-1
[58] K. Stankovic, C. Rio, A. Xia, M. Sugawara, J.C. Adams, M.C. Liberman, G. Corfas, Survival of adult spiral ganglion neurons requires erbB receptor signaling in the inner ear, J Neurosci, 24 (2004) 8651-8661. https://doi.org/10.1523/JNEUROSCI.0733-04.2004
[59] M.C. Liberman, Noise-induced and age-related hearing loss: new perspectives and potential therapies, F1000Res, 6 (2017) 927. https://doi.org/10.12688/f1000research.11310.1
[60] X. Montagutelli, Effect of the genetic background on the phenotype of mouse mutations, J Am Soc Nephrol, 11 Suppl 16 (2000) S101-105.
[61] N.A. Singh, J.F. Otto, E.J. Dahle, C. Pappas, J.D. Leslie, A. Vilaythong, J.L. Noebels, H.S. White, K.S. Wilcox, M.F. Leppert, Mouse models of human KCNQ2 and KCNQ3 mutations for benign familial neonatal convulsions show seizures and neuronal plasticity without synaptic reorganization, J Physiol, 586 (2008) 3405-3423. https://doi.org/10.1113/jphysiol.2008.154971
[62] J.F. Otto, N.A. Singh, E.J. Dahle, M.F. Leppert, C.M. Pappas, T.H. Pruess, K.S. Wilcox, H.S. White, Electroconvulsive seizure thresholds and kindling acquisition rates are altered in mouse models of human KCNQ2 and KCNQ3 mutations for benign familial neonatal convulsions, Epilepsia, 50 (2009) 1752-1759. https://doi.org/10.1111/j.1528-1167.2009.02100.x

Age Comparison (W)	S5	S20	S35	S50	S65	S80	S95
3 vs 4	0.952	0.554	0.104	0.746	0.395	0.255	0.426
3 vs 6	0.246	0.299	0.156	0.484	0.298	**0.001**	**0.04**
3 vs 8	0.157	0.070	**0.019**	0.077	**0.041**	**0.005**	**0.022**
3 vs 10	0.113	0.059	**0.005**	**0.004**	**0.035**	**$1.6x10^{-4}$**	**$8.4x10^{-4}$**
3 vs 52	**$6.0x10^{-5}$**	**$5.5x10^{-4}$**	**$2.6x10^{-4}$**	**0.001**	**$1.5x10^{-4}$**	**$3.5x10^{-6}$**	**0.001**
3 vs 58	**$1.4x10^{-5}$**	**$1.7x10^{-4}$**	**$7.2x10^{-6}$**	**$2.8x10^{-5}$**	**$1.7x10^{-5}$**	**$4.0x10^{-7}$**	**$3.2x10^{-4}$**

Table 1. Statistical analyses of OHC number for representative cochlear segments (S) in *Kcnq4*$^{-/-}$ mice. Table depicts p-values obtained from the Student's t-test comparison of the values shown in Fig. 3B. Cell number in each S, within 4W to 58W, was compared against that of 3W. Numbers in bold represent significant statistical differences.

Figure Legends

Figure 1. KCNQ4 expression in mouse cochlea

(A) Relative quantification (RQ) of *Kcnq4* mRNA was performed in the basal and middle/apical turns of 3W wild-type mouse cochleae. Total RNA was extracted and RT-qPCR was performed. The fold change of *Kcnq4* was calculated using $2^{-\Delta\Delta CT}$ and mRNA expression was referred to GAPDH and HPRT genes and compared to the basal turn. Data are represented as means ± SEM (n=3-4 pooled animals, 2 independent experiments). P<0.010 (**), Student's t-test. (**B)** Representative pictures showing immunolabeled OHCs positive for KCNQ4 in different cochlear turns at 10W. Cochlear whole-mounts were processed separately for basal, middle and apical segments and the fluorescence intensity was quantified in at least 20 cells/turn. Scale bar, 15 μm. (**C)** Mean fluorescence intensity (MFI) quantification of KCNQ4-positive cells in young adult mice. MFI values were normalized to the maximum value at each age. Signal intensity was determined for each turn using Image J program. Data are represented as means ± SEM (n=3). At 6W, ANOVA shows statistical differences between apical to basal or middle turns (p<0.001) (***). At 8W, ANOVA shows statistical differences between apical to basal (p<0.010) (**) and between apical to middle turns (p<0.010) (**). For 10W, ANOVA shows statistical differences between apical to basal (p<0.001) (***), between apical to middle (p<0.05) (*) and between middle to basal turns (p<0.001) (***).

Figure 2. OHC density in the organ of Corti of wild-type and KCNQ4 KO mice

(A) Picture of the whole cochlear extension labeled with anti-prestin (green) to identify OHCs. The entire OC length was reconstructed from 4 overlapped whole-mount fragments corresponding to the hook and basal, medial and apical turns for a 10W *Kcnq4*$^{-/-}$ mouse. The apical and basal boundaries are indicated. Dotted-white lines delimits fragments of 5% of the total OC length. Scale bar: 150 μm. (**B)** Density of OHCs for both genotypes through the whole OC length. The total number of OHCs in the entire OC was counted and expressed as a function of the total area delimited by the three OHC rows (density) in both genotypes. Data shows mean ± SEM (n=3-5). Statistically significant differences were observed among *Kcnq4*$^{-/-}$ mouse ages from 8W onwards (p<0.050, ANOVA) and for each age compared to WT animals (p<0.050, Student´s t-test). Black bars: *Kcnq4*$^{+/+}$ mice. Grey bars: *Kcnq4*$^{-/-}$ mice. Red circles represent the number of OHC present in knock-out mice compared to WT (survival ratio, right axis) at each age. (**C).** Average length of the OC for both genotypes at different ages. Color bars as indicated in B. Red circles indicate the relationship between knock-out and WT animals (Length ratio, right axis).

Figure 3. Cytocochleographical analysis of OHCs

(A) Representative pictures of wild-type (left) and KO (right) mice cochleae at 4, 10 and 52W showing OHCs abundance and arrangement in the basal, medial and apical turns. OHCs were labeled using anti-prestin (green) antibody in cochlear whole-mount preparations. Scale bar: 75 μm. Nuclei were stained with DAPI (blue). Insets show a higher magnification of the area delimited by the corresponding dashed white lines. Scale bar: 20 μm. (**B)** OHC cytocochleograms of *Kcnq4*$^{+/+}$ (left panel) and *Kcnq4*$^{-/-}$ (middle panel) mice at several ages. The number of OHC in each 5%-segment (S) of the cochlea was counted for each age, from 3W to 58W in whole-mount preparations. Each point represents mean ± SEM (n=3-5). Age is indicated in postnatal weeks (W) and symbols correspond to: 3W: black circle, 4W red inverted triangle, 6W: green square, 8W: yellow diamond, 10W: blue triangle, 40W: brown inverted triangle, 52W pink hexagon, 58W: light blue circle. Right panel depicts loss of OHC as a function of percentage distance to the apex at different ages. OHC loss was calculated as

1-(ratio of mean values between *Kcnq4*$^{-/-}$ and *Kcnq4*$^{+/+}$ mice shown in middle and left panels, respectively) for each S and age. Symbols are the same as for the other two panels. (**C)** Assessment of OHC loss rates at each segment for *Kcnq4*$^{-/-}$ mice. OHC mean counts were plotted at the indicated S vs age. Data were taken from panel B, right. Data were fitted using Hill equation (dashed lines) where nH reflects the loss rate (see Materials and Methods). Symbols for the different segments (S) are: S15: black circle, S25: red square, S40: green triangle, S55: inverted yellow triangle, S65: pink star, S75: blue diamond and S85: light blue hexagon. Open diamond and hexagon correspond to wild-type S75 and S85, respectively. (**D)** Kinetic parameters obtained from Hill's equation fittings for the corresponding segment. Hill coefficient (nH, left axis) and age where 50% OHC loss is reached (CD50, right axis) was obtained from fitting each segment, where plotted against segments. Symbols correspond to: nH: black circle, CD50: red squares.

Figure 4. OHC survival analysis for each of the three rows.
(**A)** Representative pictures showing the architecture of OHCs in the OC from *Kcnq4*$^{+/+}$ and *Kcnq4*$^{-/-}$ mice at 10W. OHCs were labeled with anti-prestin (green) and nuclei with DAPI (blue). Arrows point out missing OHCs in row 1 (red), row 2 (yellow) and row 3 (white), in *Kcnq4*$^{-/-}$ mouse. Scale bar, 25 μm. (**B)** Average OHC counts for each row in both genotypes. OHCs were counted separately for row 1 (circle), row 2 (triangle) and row 3 (square) in the S20-S60 range at different ages in wild-type (+/+) and KO (-/-) mice. Data are represented as means ± SEM from 4-5 independent experiments. For statistical analysis, each row was compared to the other 2, at each segment in both genotypes. No statistical differences were observed among rows for *Kcnq4*$^{+/+}$ animals at all ages. Asterisks indicate statistical differences between row 2 and the other two for *Kcnq4*$^{-/-}$ animals. At 6W; S25, $p<0.050$ (*) (row1 vs row2) and S50; $p<0.010$ (**) (row2 vs row3). At 8W, S25; $p<0.050$ (**) (row2 vs row3); S30, $p<0.050$ (*) (row2 vs row3); S35, $p<0.001$ (***) (row2 vs row3); S40, $p<0.050$ (*) (row2 vs row3); S45, $p<0.050$ (*) (row2 vs row3) and S55, $p<0.050$ (*) (row2 vs row3). At 10W; S30, $p<0.050$ (*) (row2 vs row3); S35, $p<0.010$ (**) (row2 vs row3); S40, $p<0.001$ (***) (row1 vs row2); S50, $p<0.010$ (**) (row2 vs row3) and S55, $p<0.010$ (**) (row2 vs row3) (ANOVA).

Figure 5. Apical surface visualization of degenerating OHCs
Scanning electron images of low (A, B, E and F) and high (C, D, G and H) magnification of OC surface in 4W (upper) and 6W (lower) mice. OHC integrity is highly conserved in WT mice (panels A and B), where internal, middle and external cell rows are indicated as 1, 2 and 3, respectively. On the contrary, in *Kncq4*$^{-/-}$ mice the absence of OHCs due to degeneration becomes apparent, as indicated by white arrows (E and F). When OHCs are observed at high magnification, stereocilia in WT mice show a neat and ordered pattern, exhibiting the characteristic W array (C and D). *Kncq4*$^{-/-}$ mice, on the other hand, exhibit a disorganized pattern with floppy stereocilia (white arrowhead), tip-fused stereocilia (yellow asterisk), or whole-fused structures (yellow arrowhead). Scale bar: 2 μm in A, B, E and F and 1 μm in C, D, G and H.

Figure 6. Cytocochleographical analysis of IHCs
(A) Representative pictures of wild-type (left) and KO (right) mice cochleae at 10 and 58W showing IHCs abundance and arrangement in the basal, medial and apical turns. IHCs were labeled using anti-myosin VIIa (red) antibody in cochlear whole-mount preparations. Scale bar: 50 μm. Nuclei were stained with DAPI (blue). Insets show a higher magnification of the area delimited by the corresponding dashed white lines. Scale bar: 10 μm. (**B)** IHC cytocochleograms of *Kcnq4*$^{+/+}$ (left panel) and *Kcnq4*$^{-/-}$ (middle panel) mice at several ages.

The number of IHC in each 5%-segment (S) of the cochlea was counted for each age, from 10W to 58W in whole-mount preparations. Each point represents mean ± SEM (n=3-5). For WT mouse, statistically significant differences were observed from S80 onwards for all ages ($p<0.050$, ANOVA). For KO mouse, statistically significant differences compared to 10W animals were observed starting at S80, S75 and S50 for 40W, 52W and 58W, respectively ($p<0.010$, Student's t-test). Age is indicated in postnatal weeks (W) and symbols corresponds to: 10W: blue triangle, 40W brown inverted triangle, 52W: pink hexagon, 58W: light blue circle. Right panel shows loss of IHC as a function of percentage distance to the apex at different ages. IHC loss was calculated as 1-(ratio of mean values between *Kcnq4*$^{-/-}$ and *Kcnq4*$^{+/+}$ mice shown in middle and left panels, respectively) for each S and age. Symbols are as for the other two panels.

Figure 7. Spiral ganglion neuron (SGN) loss in *Kcnq4*$^{-/-}$ mice

(A) Representative picture of a cochlear section showing SGN in *Kcnq4*$^{-/-}$ mice at 60W. Neurons were labeled with anti-β-III tubulin (red). White dashed lines delimit spiral ganglia area. β-III tubulin signal was superimposed on the corresponding light transmission phase contrast pictures. Abbreviations are: SV: Scala vestibuli, SM: Scala media, ST: Scala timpani, OC: Organ of Corti, LS: Limbus spiralis. Scale bar: 100 µm. (**B)** Representative pictures showing SGNs in basal and apical turns from *Kcnq4*$^{+/+}$ and *Kcnq4*$^{-/-}$ mice at 40 and 60W. β-III tubulin-positive neurons are red-colored. Corresponding phase-contrast pictures are also shown. Scale bar: 50 µm. (**C)** SGN density plot for *Kcnq4*$^{+/+}$ and *Kcnq4*$^{-/-}$ mice through age in different cochlear segments. SGN density values were obtained counting the number of β-III tubulin-positive neurons in the selected area in each segment at each age. Data are represented as means ± SEM from 3-5 independent experiments. Asterisks indicate statistical differences between *Kcnq4*$^{+/+}$ and *Kcnq4*$^{-/-}$ animals. At basal turn, $p<0.050$ (*) for 40W and $p<0.001$ (***) for 60W. At apical turn, $p<0.050$ (*) for 52W and $p<0.010$ (**) for 60W; Student´s t test.

A

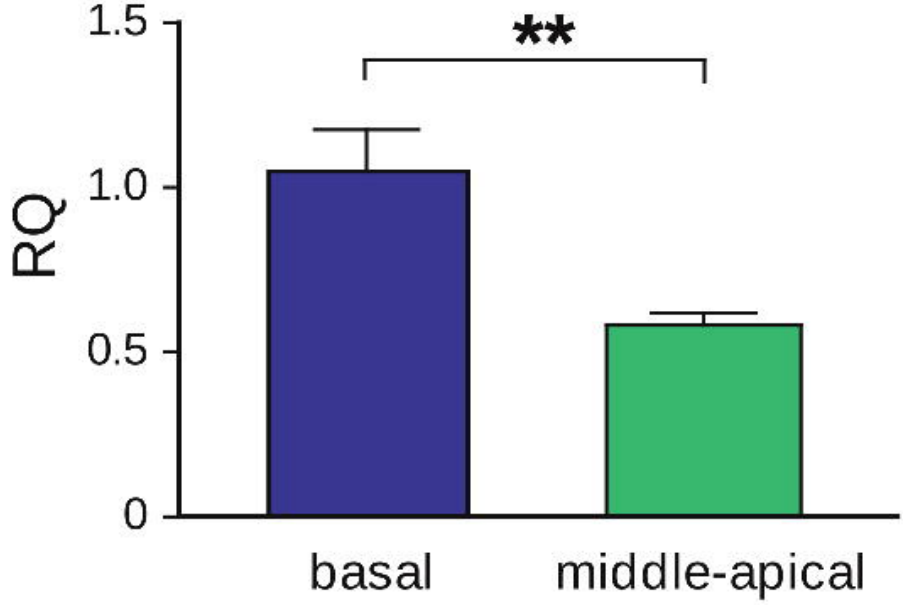
1.5
1.0
0.5
0
RQ
**
basal
middle-apical

B

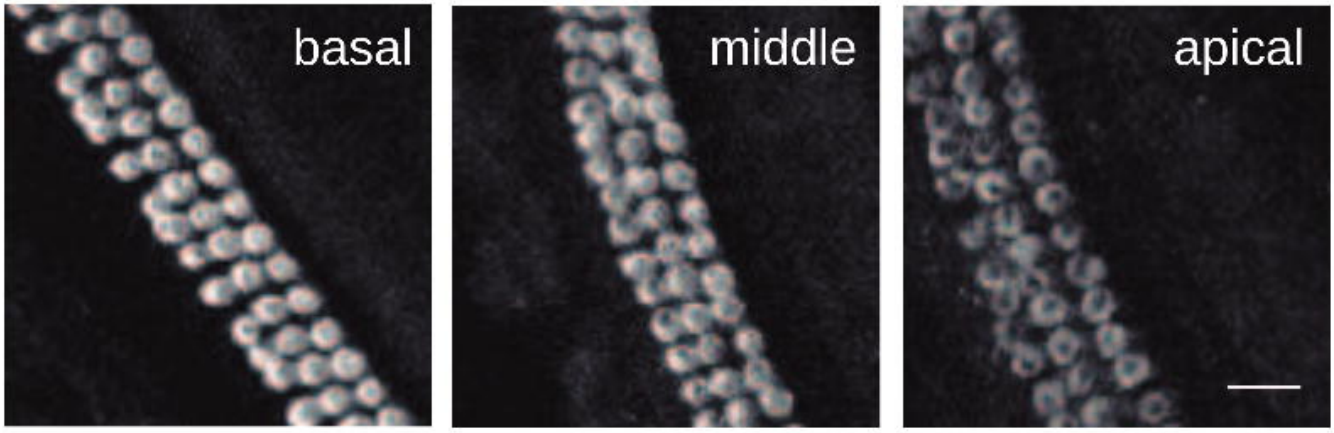
basal
middle
apical

C

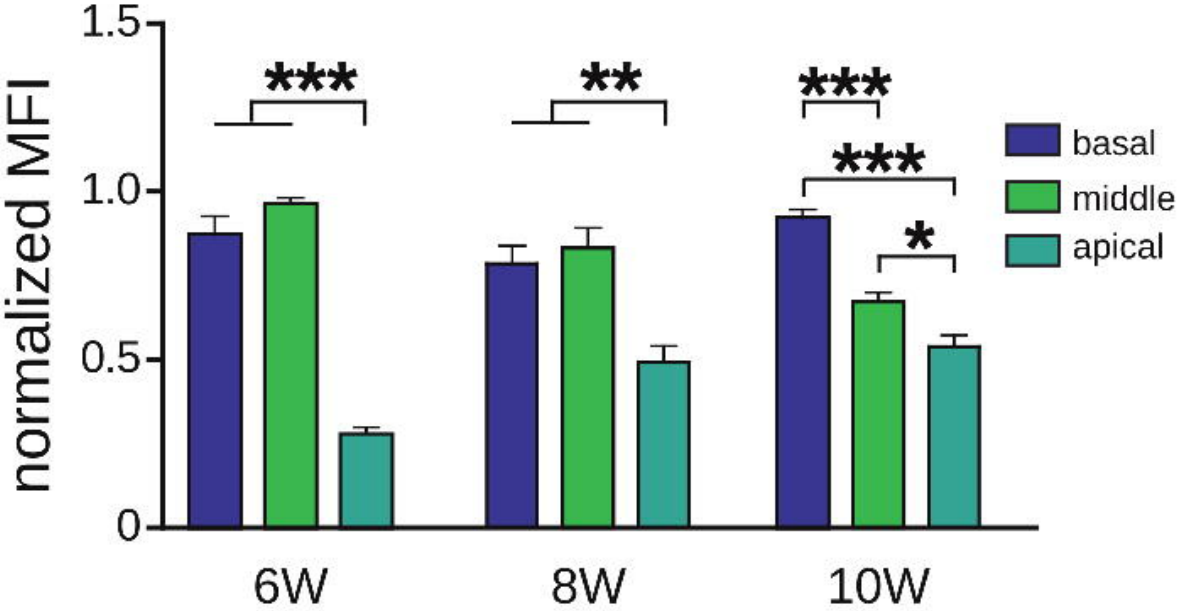
1.5
1.0
0.5
0
normalized MFI
***
**
***
***
*
basal
middle
apical
6W
8W
10W

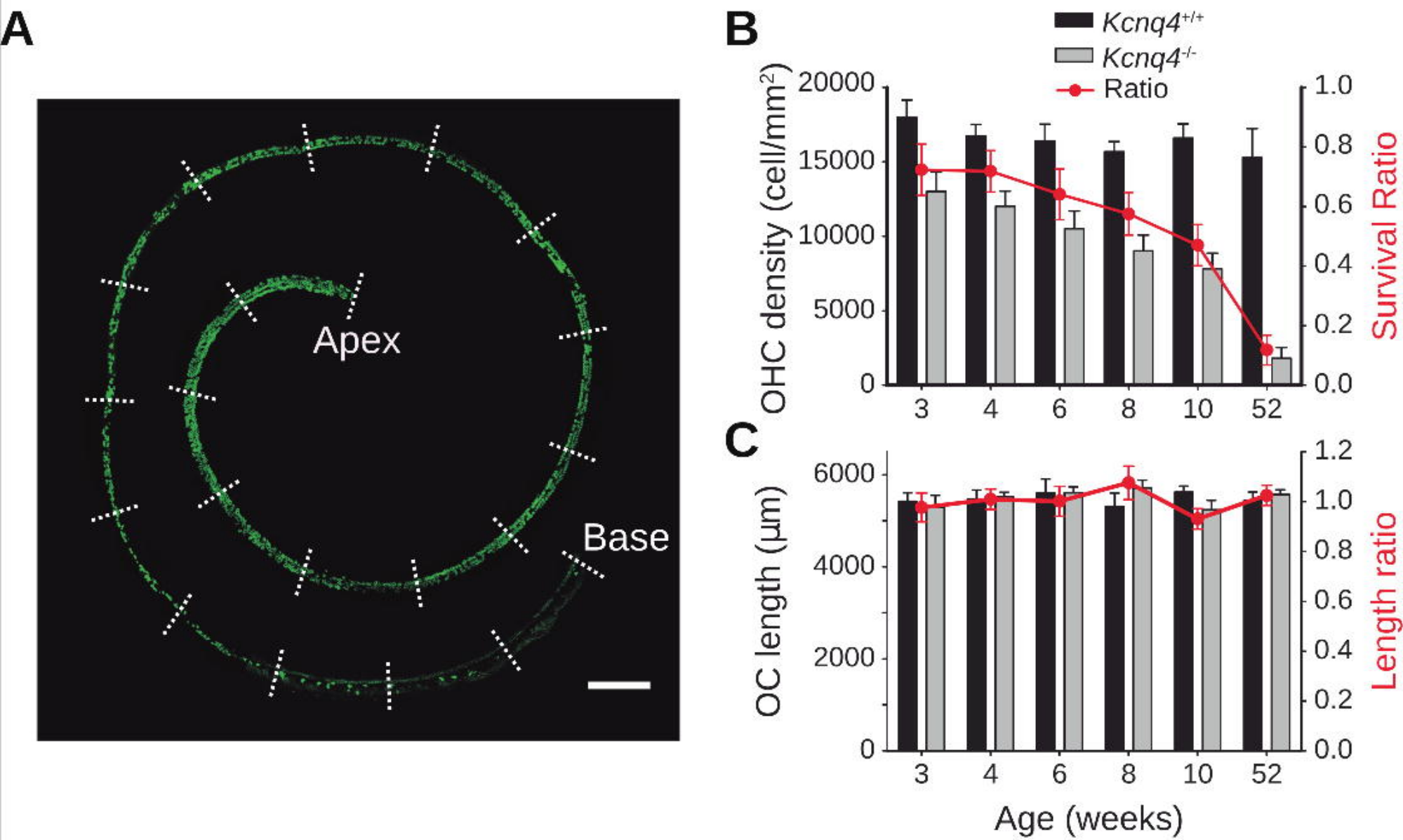
A
Apex
Base
B
Kcnq4+/+
Kcnq4-/-
Ratio
OHC density (cell/mm2)
Survival Ratio
20000
15000
10000
5000
0
1.0
0.8
0.6
0.4
0.2
0.0
3
4
6
8
10
52
C
OC length (µm)
Length ratio
6000
4000
2000
0
1.2
1.0
0.8
0.6
0.4
0.2
0.0
3
4
6
8
10
52
Age (weeks)

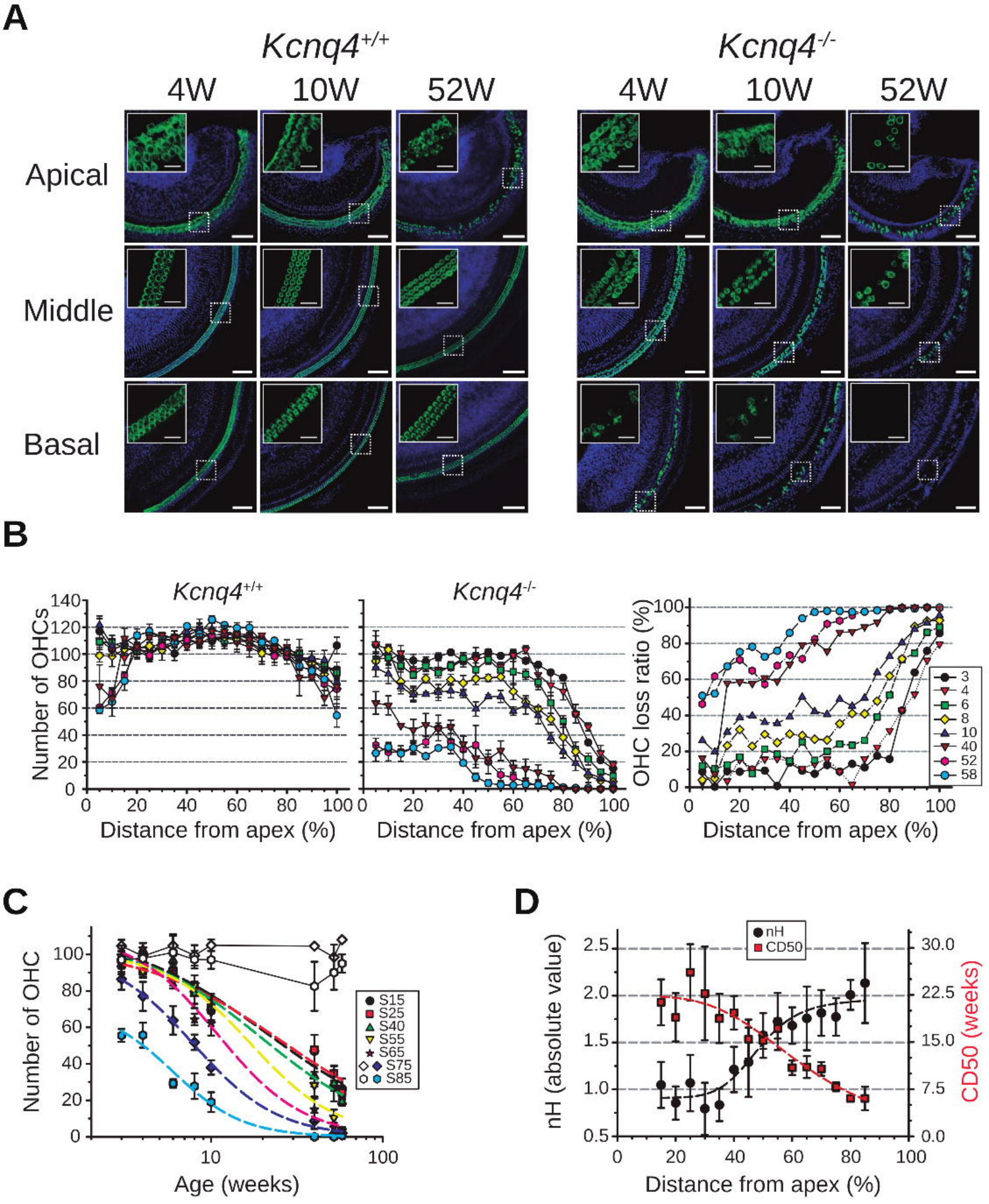
A
Kcnq4+/+
Kcnq4-/-
4W
10W
52W
Apical
Middle
Basal
B
Number of OHCs
Distance from apex (%)
OHC loss ratio (%)
3
4
6
8
10
40
52
58
C
Number of OHC
Age (weeks)
S15
S25
S40
S55
S65
S75
S85
D
nH
CD50
nH (absolute value)
CD50 (weeks)
Distance from apex (%)

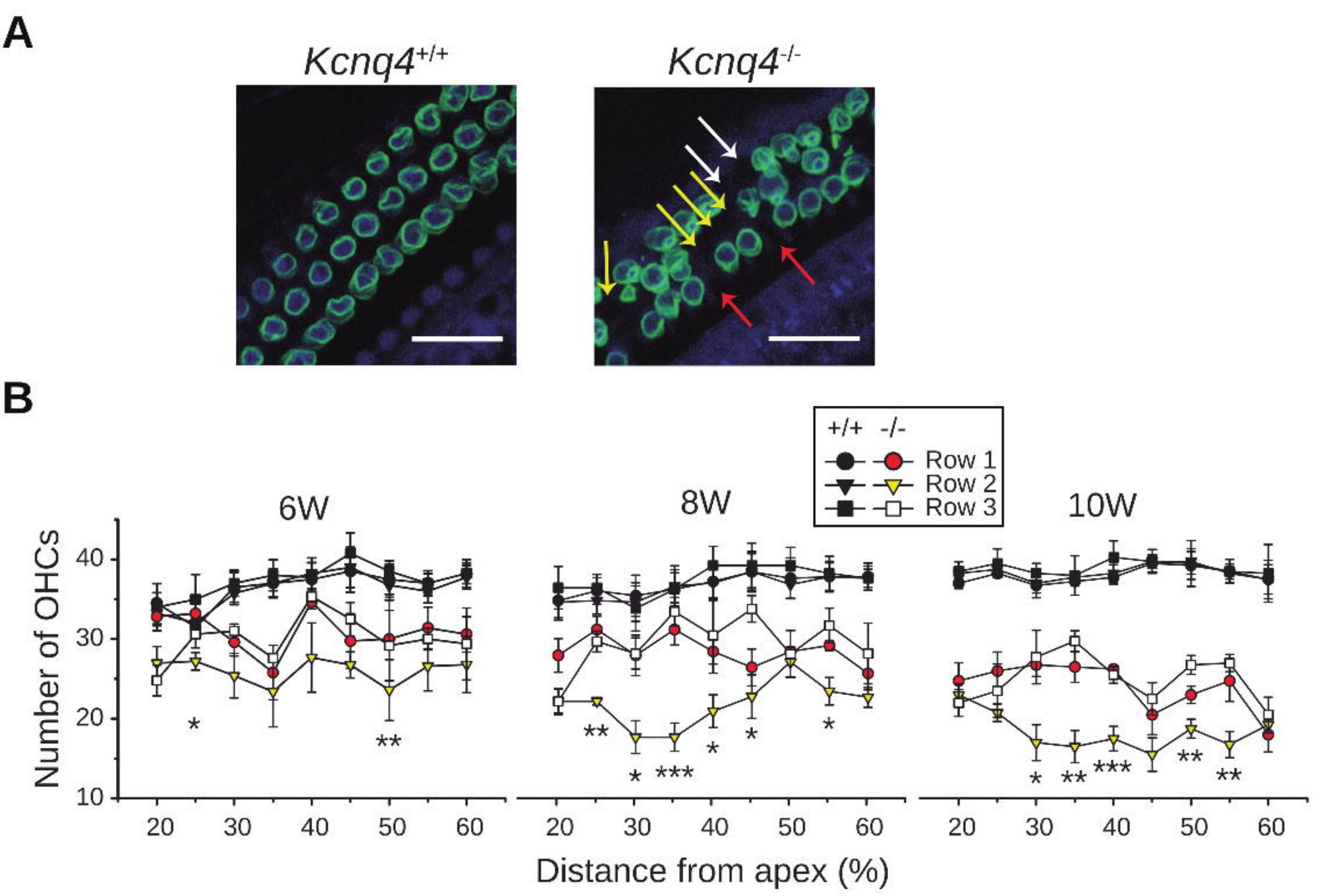
A
Kcnq4+/+
Kcnq4-/-
B
+/+ -/-
Row 1
Row 2
Row 3
6W
8W
10W
Number of OHCs
10
20
30
40
20
30
40
50
60
Distance from apex (%)
*
**
***

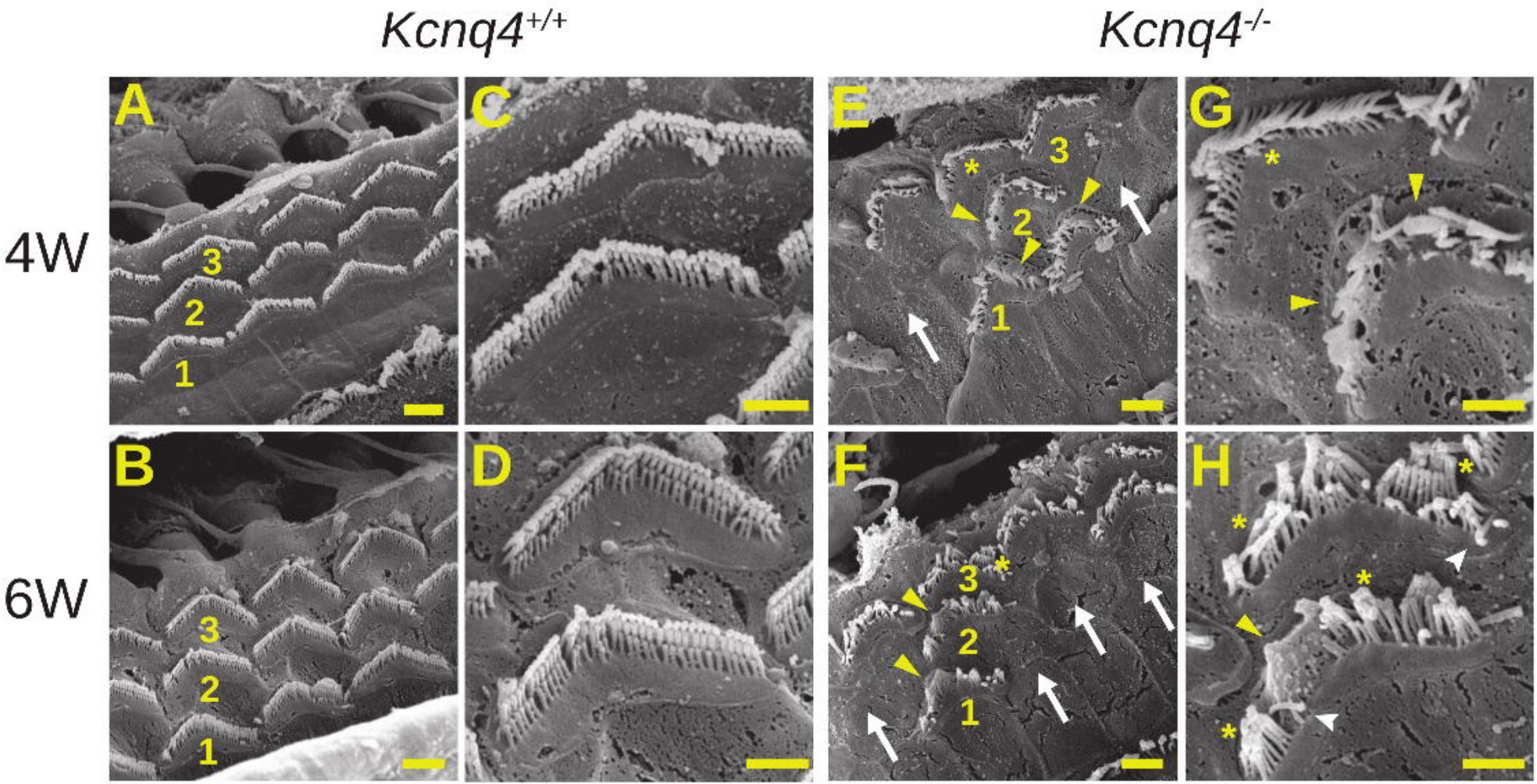
Kcnq4+/+
Kcnq4-/-
4W
6W
A
B
C
D
E
F
G
H
1
2
3
*

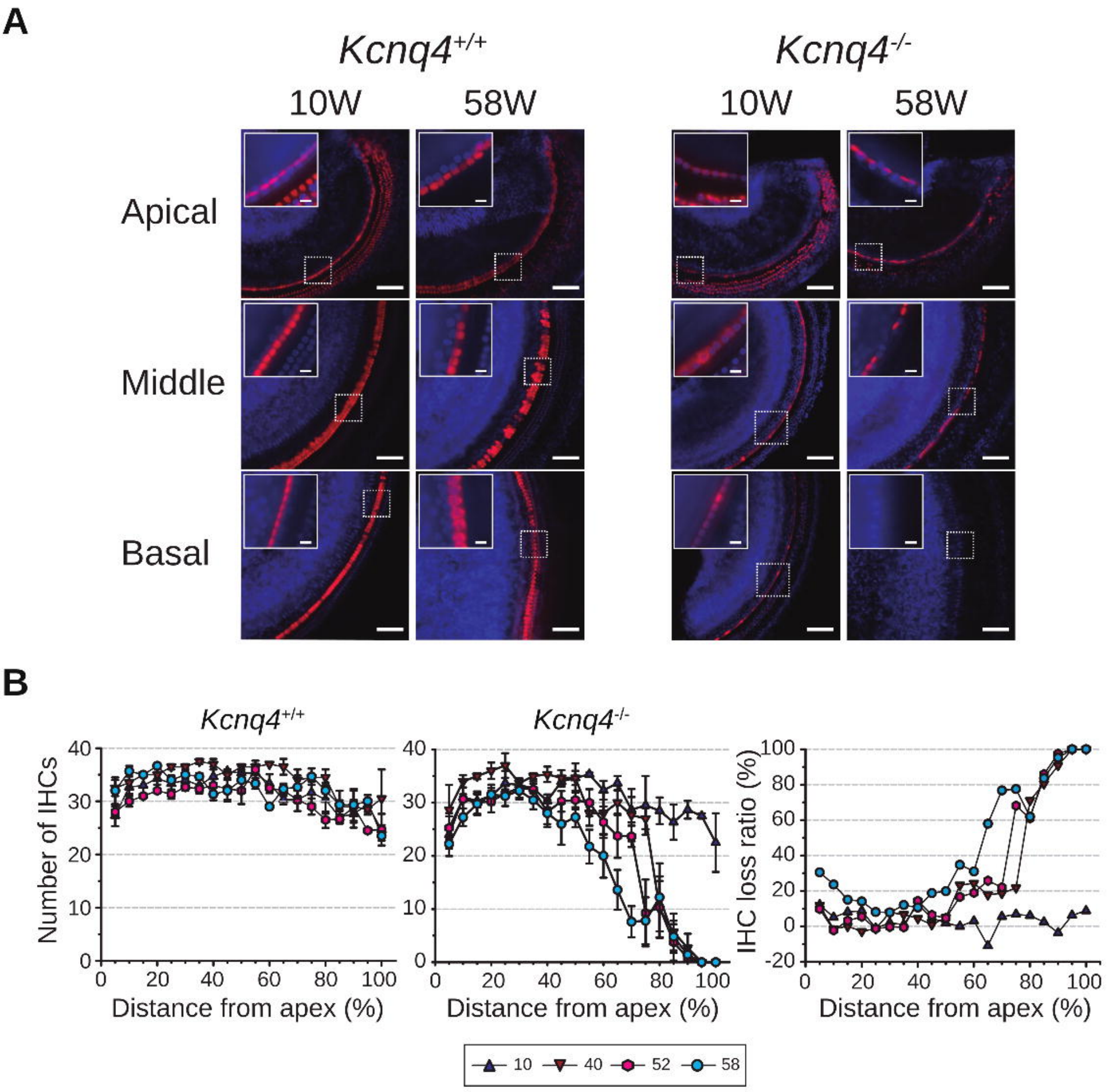
A
Kcnq4+/+
Kcnq4-/-
10W
58W
10W
58W
Apical
Middle
Basal
B
Kcnq4+/+
Kcnq4-/-
Number of IHCs
IHC loss ratio (%)
Distance from apex (%)
Distance from apex (%)
Distance from apex (%)
10
40
52
58

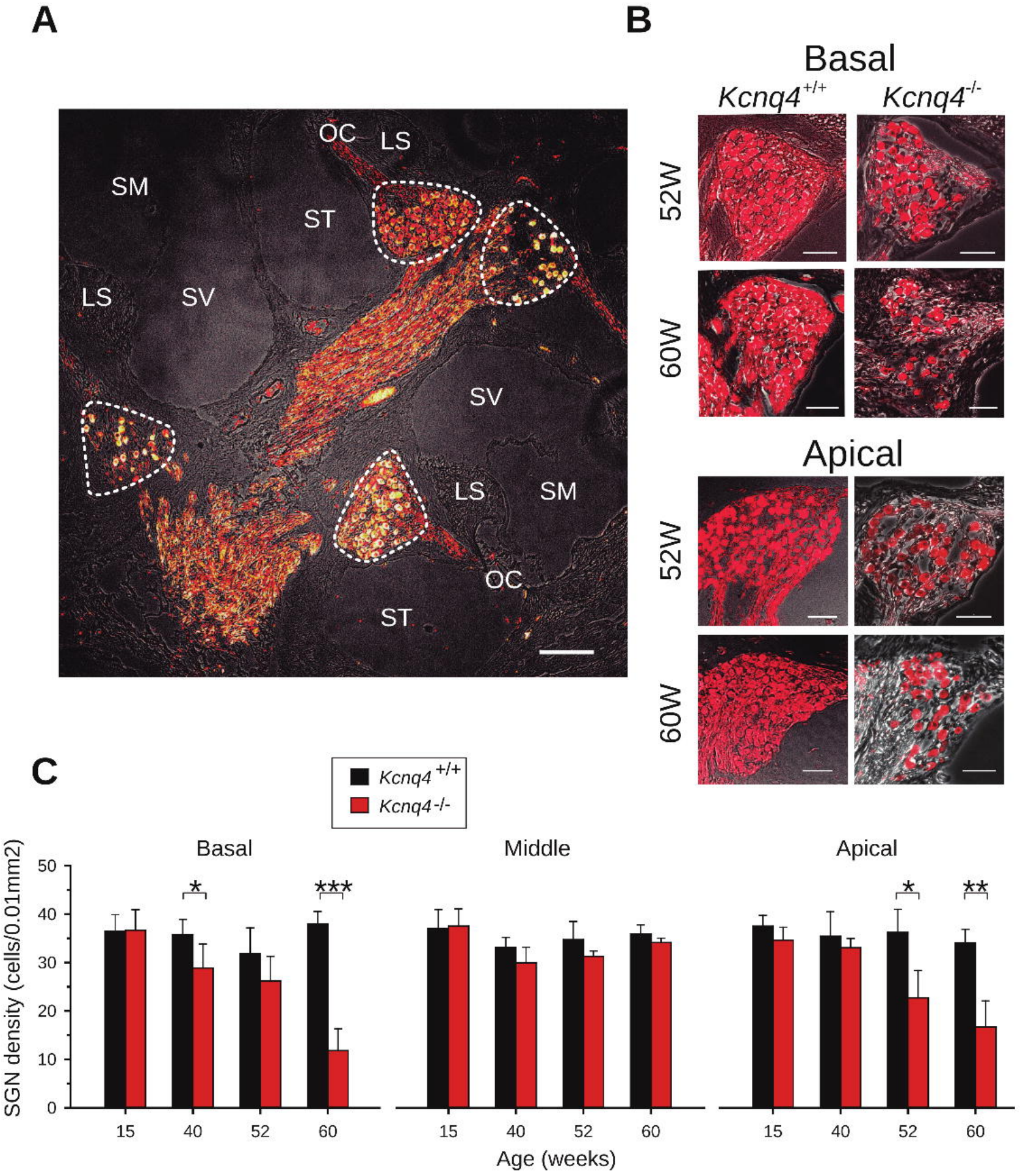
A
OC
LS
SM
ST
LS
SV
SV
LS
SM
OC
ST
B
Basal
Kcnq4+/+
Kcnq4-/-
52W
60W
Apical
52W
60W
C
Kcnq4 +/+
Kcnq4 -/-
Basal
Middle
Apical
SGN density (cells/0.01mm2)
50
40
30
20
10
0
*
***
*
**
15
40
52
60
Age (weeks)